Periodico di Mineralogia (2011), 80, 1 (Special Issue), 155-165 DOI: 10.2451/2011PM0013

PERIODICO di MINERALOGIA
established in 1930

An International Journal of
MINERALOGY, CRYSTALLOGRAPHY, GEOCHEMISTRY, ORE DEPOSITS, PETROLOGY, VOLCANOLOGY
and applied topics on *Environment*, *Archeometry* and *Cultural Heritage*

Special Issue in memory of Sergio Lucchesi

The inverse high temperature/high pressure relationship in the monoclinic $Ba_2MgSi_2O_7$ melilite-related structure

Matteo Ardit[1], Chiara Zanelli[2], Michele Dondi[2], and Giuseppe Cruciani[1,*]

[1]Dipartimento di Scienze della Terra, Università di Ferrara, Italy
[2]Istituto di Scienza e Tecnologia dei Materiali Ceramici (ISTEC - CNR), Faenza, Italy
[*]Corresponding author: *cru@unife.it*

Abstract

High-temperature study of the synthetic melilite-related $Ba_2MgSi_2O_7$ (s.g. $C2/c$) was performed up to 1273 K. Linear thermal expansion coefficients along the unit cell edges and of the volume are $\alpha_a = 8.7\times10^{-6}$ K^{-1}, $\alpha_b = 11.0\times10^{-6}$ K^{-1}, $\alpha_c = 8.5\times10^{-6}$ K^{-1}, and $\alpha_V = 31.1\times10^{-6}$ K^{-1}, respectively, showing an anisotropic expansion behaviour characterized by $\alpha_a \approx \alpha_c < \alpha_b$. High-temperature data were then combined with high-pressure data (taken from the literature) for the same monoclinic sample. The "*inverse relationship*" of variation against temperature and pressure is observed for both the unit cell parameters and the (c/a) axial ratio as a function of the molar volume. A further comparison with melilite-type compounds at ambient condition along the join $(Ca\text{-}Sr\text{-}Ba)_2MgSi_2O_7$ reveals that the tetragonal polymorph of the barium compound ($Ba_2MgSi_2O_7$) should be a metastable phase favoured by high pressure conditions.

Key words: melilite-related structures; melilite-type structures; "inverse relationship"; high-temperature; high-pressure; comparative crystal chemistry.

Introduction

Solved in 1984 by Malinovskii, the monoclinic $Ba_2CuSi_2O_7$ (s.g. $C2/c$ and $Z = 4$) is the archetype form for $Ba_2T1Si_2O_7$ melilite-related compounds. Other silicates with this structure include $Ba_2CoSi_2O_7$ (Adams et al., 1996), $Ba_2ZnSi_2O_7$ (Kaiser and Jeitschko, 2002), and $Ba_2MgSi_2O_7$ (Aitasalo et al., 2006). Although suggested as structures that should not crystallize with a tetragonal melilite-type structure (Rothlisberger et al., 1990), the above listed Mg, Co, and Cu melilite-related compounds were also solved in the $P\bar{4}2_1m$ space group (Z = 2): $Ba_2MgSi_2O_7$ (Shimizu et al.,1996), $Ba_2CoSi_2O_7$ (El Bali and Zavalij, 2003), and $Ba_2CuSi_2O_7$ (Du et al., 2003) single crystals were successfully refined as melilite-type compounds.

Although with the same stoichiometry ($Ba_2T1Si_2O_7$), the monoclinic and tetragonal polymorphs exhibit substantial differences. Similarly to the extensively studied melilite-type

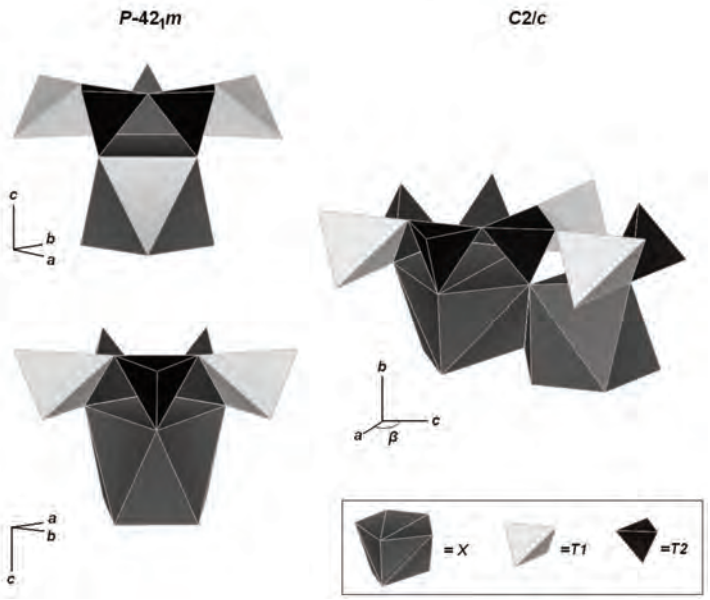

Figure 1. Eight-coordinated Ba cation in melilite-type (on the left) and melilite-related (on the right) compounds.

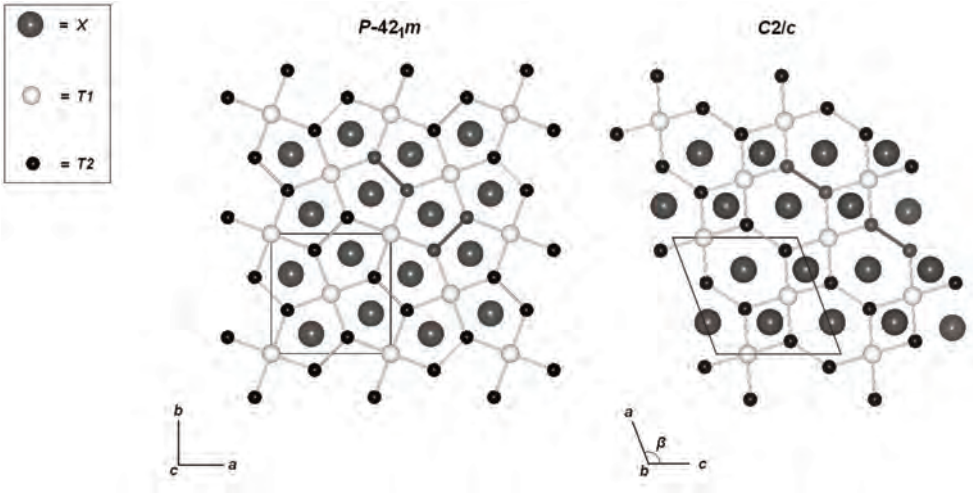

Figure 2. Layer topologies along [001] for melilite-type (on the left) and along [010] for melilite-related (on the right) structures. The different arrangement of the Si_2O_7 dimers for the two topologies are given by highlighted Si–Si bonds.

structures, the monoclinic polymorphs consist of Si_2O_7 dimers connected by $T1O_4$ tetrahedra to form tetrahedral sheets parallel to the *ac* plane, instead of the *ab* plane in the $P\bar{4}2_1m$ structure. The first major difference concerns the coordination polyhedron of the barium cation, that in the tetragonal feature is a distorted square antiprism with "4 above + 4 below" ligands, whereas in the monoclinic form it is an alternation of "5+3" and "3+5" ligand configuration (see Figure 1).

However, as already pointed out by Armbruster et al. (1990), the main difference is in the arrangement of the tetrahedral sheet topology (see Figure 2): there are only five-membered rings of tetrahedra in the tetragonal form, while four- and six-membered rings are present in the monoclinic structure. The change in the tetrahedral sheet arrangement promotes a new setting of the Si_2O_7 dimers laying in the same layer: in the melilite-type dimers are alternatively disposed along (110) and ($\bar{1}$10), whereas in the melilite-related compounds all the dimers are arranged along ($\bar{1}$01).

In the last decade, many studies were dedicated to assess the high- and low-temperature behaviour of melilite-type structures, especially to interpret and solve the phase transition from an incommensurately modulated (IC) to a normal (N) crystal structure occurring in melilite-type compounds with calcium occupying the eight-fold coordinated *X* site (e.g. Hemingway et al., 1986; Webb et al., 1992; Riester and Böhm, 1997; McConnell et al., 2000; Kusaka et al., 2001; Bagautdinov et al., 2002; Merlini et al., 2005; Merlini et al., 2008). On the other hand, few works have been devoted to understand the high-pressure response of melilite structures (e.g. Yang et al., 1997; Haussühl and Liebertz, 2004; Merlini et al., 2009), and no studies have been done about melilite-related compounds at non-ambient conditions.

In this paper, data on the thermal expansion of $Ba_2MgSi_2O_7$ melilite-related compound up to 1273 K and its structural response are presented. Furthermore, high-temperature data are combined with high-pressure data (Ardit et al., 2011) in order to test the "*inverse relationship*" between structural variations due to temperature versus pressure (Hazen and Finger, 1982), and to better understand the difference occurring between the two polymorph families.

Experimental

Sample synthesis

Reagent grade $BaCO_3$, MgO and SiO_2 were used as raw materials to prepare the polycrystalline $Ba_2MgSi_2O_7$ compound by a solid state reaction, following the process of wet mixing of raw materials, drying in oven, pulverization in agate mortar, then calcination in alumina crucible in an electric kiln in static air at maximum temperature of 1200 °C for several hours by applying a heating rate of 3 °C·min^{-1}.

Data collection at ambient conditions and refinement strategy

X-ray powder diffraction measurement at ambient conditions was performed by a Bruker D8 Advanced equipped with a Si (Li) solid-state detector, set to discriminate Cu $K\alpha_{1,2}$ radiation, in the 15-130° 2θ measuring range, with a counting time of 10 s per 0.02° 2θ step.

The structural refinement was run by the Rietveld method using the GSAS-EXPGUI software packages (Larson and Von Dreele, 1988; Toby, 2001). In addition to the almost pure $Ba_2MgSi_2O_7$ melilite-related compound, a small amount of barium silicate ($BaSiO_3$) was detected, but quantitative Rietveld analysis indicates it is a minor phase with a mass fraction of ~ 4.7%. The presence of such minor compound was accounted for by running a multiphase refinement in which only the scale factor and the cell parameters were varied for the $BaSiO_3$ phase.

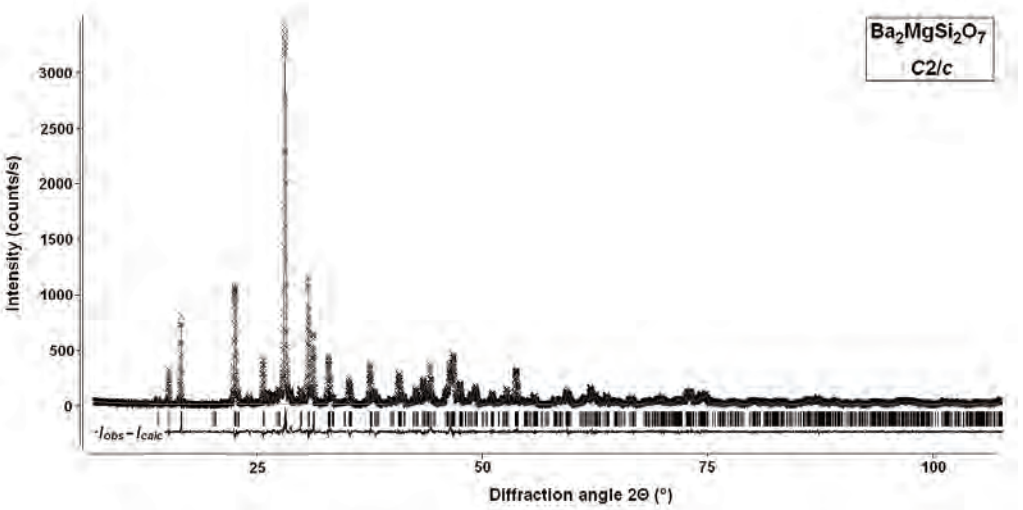

Figure 3. Plot of the Rietveld fitting of $Ba_2MgSi_2O_7$ melilite-related (s.g. *C*2/*c*) at ambient condition. The experimental data are indicated by crosses, the calculated pattern is the continuous line (among the crosses) and the lower curve is the weighted difference between the calculated and observed patterns. Vertical ticks mark the position of reflections for melilite phases.

Table 1. Comparison of selected parameters for $Ba_2MgSi_2O_7$ melilites-related (s.g. *C*2/*c*) at ambient condition. Unit cell parameters, mean metal-oxygen bond distances, polyhedral volumes, mean interatomic angles, and their standard deviations (in parentheses) are listed.

	$Ba_2MgSi_2O_7$ (this study)	**$Ba_2MgSi_2O_7$** (Aitasalo et al., 2006)
Unit cell parameters		
a (Å)	8.4171(3)	8.4128(1)
b (Å)	10.7194(4)	10.7101(1)
c (Å)	8.4501(3)	8.4387(1)
β (°)	110.77(1)	110.71(1)
V (Å^3)	712.89	711.21
Mean metal-oxygen bond length (Å)		
⟨Ba–O⟩	2.820(12)	2.813(8)
⟨Mg–O⟩	1.966(3)	1.965(9)
⟨Si–O⟩	1.629(5)	1.630(8)
Polyhedral volume (Å^3)		
V_{BaO8}	33.41	33.19
V_{MgO4}	3.78	3.80
V_{SiO4}	2.19	2.19
Mean interatomic angles (°)		
⟨O–Si–O⟩	109.3(7)	109.2(5)
⟨Mg–O–Si⟩	117.5(5)	117.6(4)

Starting atomic model was taken from the single-crystal refinement of Adams et al. (1996) in the space group *C*2/*c*, with Mg replacing Co. The diffraction peak profile was modelled by a pseudo-Voigt function with one Gaussian and two Lorentzian broadening coefficients plus an asymmetry contribution. Besides the 18 shifted Chebyshev polynomial coefficients to reproduce the background, the refinements included a scale factor, cell parameters, final atomic coordinates, and isotropic atomic displacement parameters, leading to an $R_{wp} = 0.1546$, $R_p = 0.1128$, and $R_F^2 = 0.0267$ for 1165 independent nonzero reflections in the collecting range. During the refinement of the atomic coordinates, a soft constraint was applied to the Si–O distances (i.e. Si–O1 = Si–O2 = 1.660 ± 0.010 Å, and Si–O3 = Si–O4 = 1.600 ± 0.005 Å), with the constraint weight being progressively lowered until a minimal value. The plot of the Rietveld refinement is reported in Figure 3. The data obtained from this structural refinement and those previously reported by Aitasalo et al. (2006) for a same polycrystalline compound, are reported in Table 1 for comparison.

High-temperature data collection and refinement strategy

High temperature X-ray powder diffraction study of the monoclinic $Ba_2MgSi_2O_7$ was carried out using a Bruker D8 Advanced equipped with a 1-dimensional LynxEye, and a hot chamber (MRI BASIC) with a Type-S thermocouple (Pt/Pt10Rh). A small amount of the sample, previously mixed with a 15% in weight of CeO_2 (National Bureau of Standards, Gaithersburg, Maryland, USA), was mounted on a Pt20Rh stage-heating element. Cerium oxide was selected as internal standard for temperature calibration because no peaks of its cubic lattice overlap with those of our sample, and because CeO_2 is an extensively studied material at high-temperature conditions, and the volumetric and lattice parameter thermal expansion are determined with extreme accuracy (e.g. Körner et al., 1989; Shuk and Greenblatt, 1999; Sameshima et al., 1999; Mathews et al., 2000; Chavan et al., 2003; Chavan et al., 2004; and many others). The XRD patterns were recorded every 100°C from ambient temperature to 1000°C in air with a heating rate of $0.17°C \cdot s^{-1}$ in the 10-80° 2θ range, with a counting time of 0.5 s per 0.02° 2θ step.

While the line positions in the powder patterns were accurately determined with the above experimental set-up, the measured line intensities were not accurate enough to allow a series of full structure refinements due to the 'infinitively-thick-sample' condition not being met. Therefore, the structural model refined for monoclinic $Ba_2MgSi_2O_7$ at ambient conditions was used and kept fixed for all the temperature steps of the high-temperature measurements. Besides the unit cell parameters, all Rietveld refinements included one Gaussian and two Lorentzian broadening coefficients of the pseudo-Voigt function to model the peak profiles, a sample-shift contribution to account for its changing height with respect to the focussing circle, and 20 Chebyshev polynomial coefficients to reproduce the background.

Result and discussion

The lattice parameters *a*, *b*, *c*, *β*, the unit cell volume *V*, and the thermal expansion coefficients (*TECs*) for the monoclinic $Ba_2MgSi_2O_7$ in the temperature range 303-1273 K are reported in Table 2. The coefficients of thermal expansion are given by

$$\alpha_l(T) = 1/l(\partial l / \partial T)_{X,P} \quad (1)$$

with composition and pressure held constants.

Normalized unit-cell axes and volume plotted in Figure 4 scale linearly with increasing temperature. As expected from its layered nature, $Ba_2MgSi_2O_7$ does not exhibit an isotropic expansion behaviour (which would imply $\alpha_V \approx$

$3\alpha_{edge}$), but is characterized by $\alpha_a \approx \alpha_c < \alpha_b$, namely the thermal expansion coefficient along the *b*-axis is higher than those along the tetrahedral layers which are almost equal. The same anisotropy is commonly found in melilite-type compounds studied under high-temperature, that always show a higher coefficient of thermal expansion perpendicularly to the tetrahedral layers.

In numerous crystalline materials, structural changes are mainly function of the molar volume. For these materials, the structural answers with decreasing temperature are the same to those with increasing compression (i.e. the so-called "*inverse relationship*" previously described by Hazen and Finger, 1982). Therefore, it is interesting to compare the measured high-temperature data with those recently collected and described under high-pressure conditions by Ardit et al. (2011) for the melilite-related $Ba_2MgSi_2O_7$ compound.

In Figure 5 is reported the variation of the normalized lattice parameters (a/a_0, b/b_0 and c/c_0) as a function of the normalized cell volume (V/V_0). For these parameters an almost ideal inverse relationship exists and both the pressure and temperature data sets describe almost linear trends along the same parameter.

The *c*/*a* axial ratio is a common way to estimate the anisotropy among the three orthogonal dimensions of the unit cell in tetragonal melilite-type compounds, relating the tetrahedral layer corrugation (out of the *ab*-plane) with the dimension of the cation in the *X* site (along the *c*-axis). In order to obtain a similar and meaningful value also for the monoclinic melilite-related compounds we propose the $(c/a)^*$ axial ratio where: $c^*=b_{mon.}/2$ and $a^*=\sqrt{a_{mon.}\times c_{mon.} sen\beta}$. The resulting values of a such calculated $(c/a)^*$ ratio are plotted in Figure 6 as a function of the normalized cell volume (V/V_0). Even if the inverse relationship is still maintained, the high-pressure/high-temperature data sets show two distinct trends. The evolution of the axial ratio clearly highlights the subtle difference which exists and is expected in the anisotropic response of the melilite-related lattice towards high pressure vs. high temperature conditions.

Table 2. Thermal expansion data for the monoclinic $Ba_2MgSi_2O_7$, and their standard deviations (in brackets).

T (K)	*a* (Å)	*b* (Å)	*c* (Å)	*β* (°)	*V* (Å^3)	*(c/a)**
303	8.4144(5)	10.7165(5)	8.4475(5)	110.76(1)	712.27(8)	0.6572(1)
373	8.4188(5)	10.7246(5)	8.4520(5)	110.73(1)	713.71(8)	0.6573(1)
473	8.4257(5)	10.7363(5)	8.4592(5)	110.68(1)	715.91(8)	0.6574(1)
573	8.4344(5)	10.7492(5)	8.4675(5)	110.64(1)	718.42(8)	0.6574(1)
673	8.4422(5)	10.7609(5)	8.4740(5)	110.59(1)	720.63(8)	0.6575(1)
773	8.4489(5)	10.7726(5)	8.4817(5)	110.55(1)	722.86(9)	0.6575(1)
873	8.4562(5)	10.7841(5)	8.4891(5)	110.51(1)	725.08(9)	0.6576(1)
973	8.4642(5)	10.7955(6)	8.4964(5)	110.47(1)	727.34(9)	0.6576(1)
1073	8.4704(6)	10.8071(6)	8.5034(6)	110.43(1)	729.45(9)	0.6577(1)
1173	8.4773(6)	10.8182(6)	8.5104(6)	110.38(1)	731.62(10)	0.6577(2)
1273	8.4857(6)	10.8316(6)	8.5178(6)	110.35(1)	734.06(10)	0.6579(2)
TEC ($\alpha \times 10^{-6}$ K^{-1})	*8.67(3)*	*11.01(4)*	*8.51(3)*		*31.05(9)*	

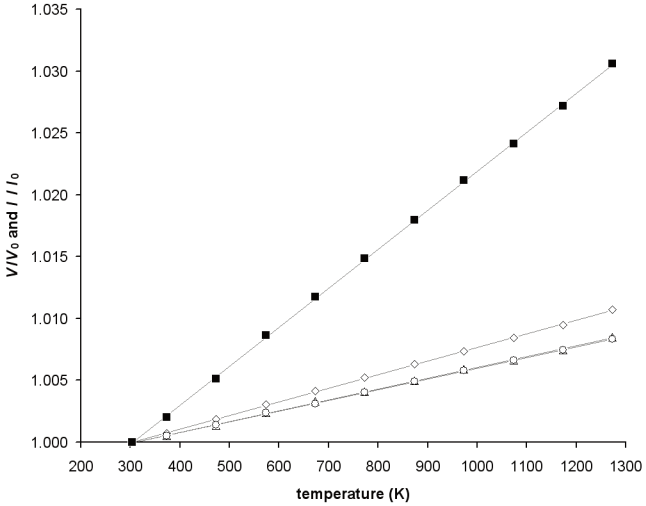

Figure 4. Unit cell volume (V/V_0: black filled squares) and lattice parameters (a/a_0: triangles; b/b_0: diamonds; and c/c_0: circles) of $Ba_2MgSi_2O_7$ melilite-related compound as a function of temperature. Lines through data-points are the fitting curves obtained from eq. 1 and TECs in Table 2.

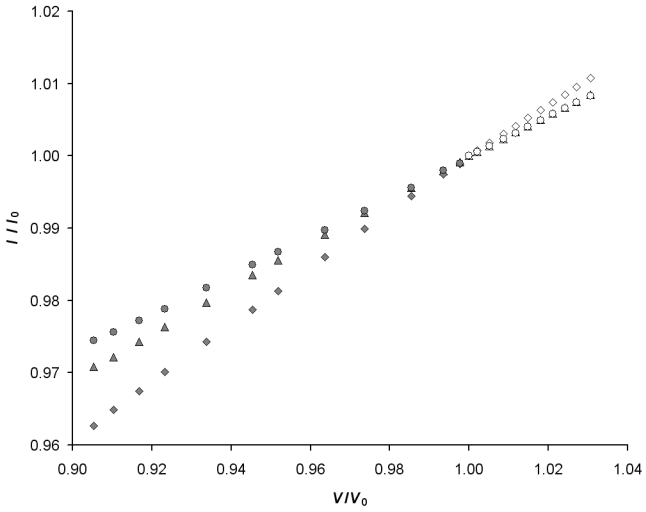

Figure 5. Almost ideal inverse relationship with pressure (grey filled symbols) and temperature (empty symbols), characterized by the continuous variation of the lattice parameters ($a/a_0 = b/b_0$: triangles; c/c_0: circles) versus V/V_0.

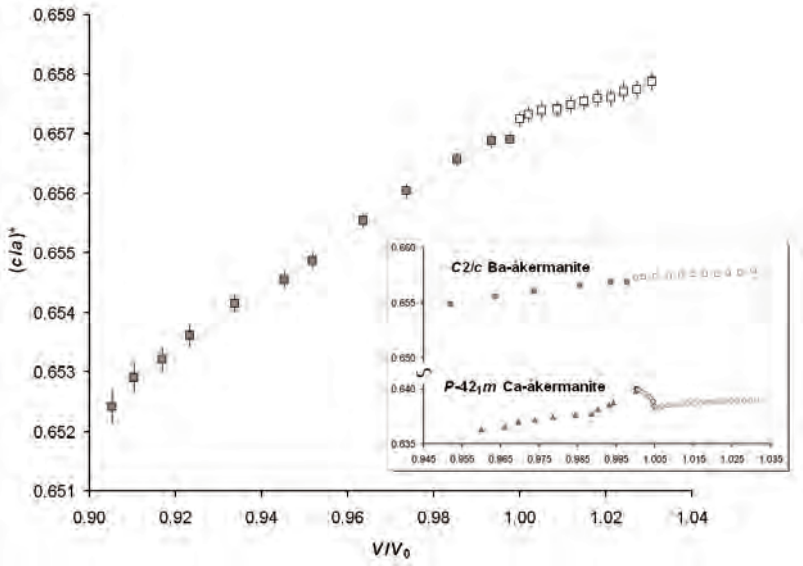

Figure 6. The inverse relationship for the monoclinic $Ba_2MgSi_2O_7$. Plot of the (c/a)* ratio versus normalized volume V/V_0 (pressure; grey filled symbols; temperature: empty symbols). The inset shows the comparison with the tetragonal Ca-åkermanite structure (HP and HT data from Yang et al., 1997 and Merlini et al., 2005, respectively). The two trends have very similar linear slopes, except within the region where Ca-åkermanite behaves as an incommensurately modulated structure.

The axial ratio in melilite-type (c/a) and related structures $(c/a)^*$ also varies as a function of the composition as described by the T/X dimensional misfit parameter. The latter is calculated as the ratio of the average tetrahedral bond distances over the $\langle X–O\rangle$ bond distances and reflects the geometrical constraints existing on the ratio of ionic radii of T and X cations for the occurrence of stable melilite-type structures. Therefore, the T/X parameter best defines the compositional field of existence for the different kinds of $X_2T1T2_2A_7$ compounds (e.g. Rothlisberger et al., 1990). The relationship between $(c/a)^*$ and T/X is illustrated in Figure 7 considering Ca- and Sr-åkermanites (tetragonal symmetry), the (Ba, Sr) solid solution term, which marks the transition from tetragonal to monoclinic symmetry (Ardit et al., 2011), and both monoclinic and tetragonal $Ba_2MgSi_2O_7$. We suggest that when moving along this trend from the high T/X and low $(c/a)^*$ region [i.e. $T/X >$ 0.627 and $(c/a)^* < 0.654$] to lower T/X and higher $(c/a)^*$, the $X_2MgSi_2O_7$ compounds are no longer stable with tetragonal symmetry (i.e. with melilite-type structure) and are favoured to adopt the monoclinic $Ba_2CuSi_2O_7$-type structure. It must be pointed out that, while the tetragonal Ca-, Sr- and $(Ba_{1.6}Sr_{0.4})$-åkermanites, and the monoclinic $Ba_2MgSi_2O_7$ are stable forms which can be synthesized by solid state reactions, the tetragonal polymorph of $Ba_2MgSi_2O_7$ is a metastable form only obtained from melt crystallization under very carefully controlled conditions (Shimizu et al., 1995).

The above considerations allow some speculations to be made on the possible occurrence of a phase transition from monoclinic to lower (triclinic) or higher (e.g. tetragonal)

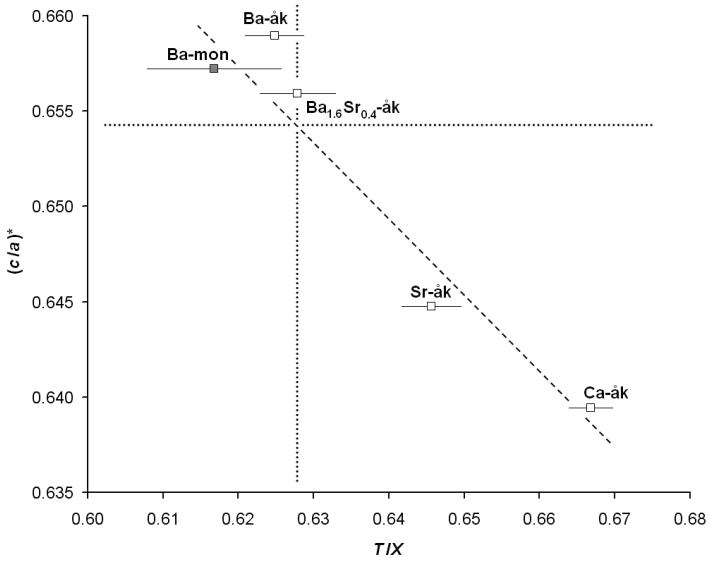

Figure 7. $(c/a)^*$ ratio as a function of the *T/X* ratio (see text for explanation). Grey filled symbol refers to the structure studied in this work. Empty symbols and labels are as follows: [Ca-åk] = $Ca_2MgSi_2O_7$ Kimata and Ii, 1981; [Sr-åk] = $Sr_2MgSi_2O_7$ and [$Ba_{1.6}Sr_{0.4}$-åk] = ($Ba_{1.6}Sr_{0.4}$)$MgSi_2O_7$ Ardit et al., 2011; [Ba-åk] = $Ba_2MgSi_2O_7$ Shimizu et al., 1995.

symmetry induced by pressure or temperature in $Ba_2MgSi_2O_7$. If the $(c/a)^*$ limit of ~ 0.654 is taken as a boundary at which the changes of *T*/*X* dimensional misfit affects the relative stabilities of the monoclinic vs. tetragonal structure, then we expect that such a limit might also be reflected by a discontinuity on the trend of $(c/a)^*$ as a function of pressure and temperature. As a matter of fact, a careful inspection of Figure 6 reveals a subtle jump at about $(c/a)^* = 0.6545$ which occurs on the compression side. Examination of powder patterns around this value does not provide any indication for the occurrence of a phase transition. On the other hand, due to kinetic hindrances, it is unlikely that a reconstructive transformation as the one relating the layer topology of the two $Ba_2MgSi_2O_7$ polymorphs would take place under high pressure conditions at room temperature.

Concerning the structural reasons why the tetragonal polymorph should be favoured by high pressure, besides the reduced dimensional misfit between the tetrahedral layer and the interlayer, we note that the most significant difference in the bond distances of the two $Ba_2MgSi_2O_7$ polymorphs is in the average ⟨Ba–O⟩ distance. In fact, ⟨Ba–O⟩ is equal to 2.793 Å for the tetragonal form (Shimizu et al., 1995) while is 2.820 Å in the monoclinic form (Ardit et al., 2011). Furthermore, the monoclinic structures of $Ba_2T1Si_2O_7$ compounds (*T1* = Mg, Co, Zn, Cu) do not show Ba–O distances less then ~ 2.69 Å, while bond distances down to 2.648 Å and 2.627 Å are found in tetragonal $Ba_2MgSi_2O_7$ (Shimizu et al., 1995) and $Ba_2CoSi_2O_7$ (El Bali and Zavalij, 2003), respectively. In other words, the Ba coordination environment in the tetragonal polymorph would

be strongly favoured by high pressure compared to the monoclinic situation.

We also argue that the more intuitively conceivable transition from monoclinic to tetragonal at high temperature would never occur, as a solid state transformation, because Figure 6 clearly shows that the $(c/a)^*$ axial ratio increases with temperature, leading to T/X misfit values which are not compatible with the tetragonal melilite structure (Figure 7). This observation explains the many unsuccessful attempts we made in order to obtain the tetragonal phase by heating the synthesized monoclinic powder at high temperatures.

As a final remark, the present study represents a nice application of the comparative *P-T-X* (pressure-temperature-composition) approach in the sense of Hazen and Finger (1982).

Acknowledgements

This paper is to honour late Prof. Sergio Lucchesi. One of us (G.C.), while PhD student at the University of Perugia, met him for the first time during a visit Sergio paid to improve his skills in single crystal diffraction. Sergio's claim that crystallography is the most powerful tool in mineral sciences still holds as a living memory of him. We are very grateful to Fernando Camara and to an anonymous referee for the critical reading of manuscript.

References

Adams R., Layland R., Payen C. and Datta T. (1996) - Syntheses, structural analyses, and unusual magnetic properties of $Ba_2CoSi_2O_7$ and $BaCo_2Si_2O_7$. *Inorganic Chemistry*, 35, 3492-3497.

Aitasalo T., Hölsä J., Laamanem T., Lastusaari M., Letho L., Niittykoski J. and Pellé F. (2006) - Crystal structure of the monoclinic $Ba_2MgSi_2O_7$ persistent luminescence material. *Zeitschrift für Kristallographie Suppl*., 23, 481-486.

Ardit M., Cruciani G. and Dondi M. (2011) - Melilite-type and melilite-related compounds: structural variations along the join $Sr_{2-x}Ba_xMgSi_2O_7$, ($0 \le x \le 2$) and high-pressure behaviour of the two end-members. Submitted to *Physics and Chemistry of Minerals.*

Armbruster T., Röthlisberger F. and Seifert F. (1990) - Layer topology, stacking variation, and site distortion in melilite-related compounds in the system CaO-ZnO-GeO_2-SiO_2. *American Mineralogist*, 75, 847-858.

Bagautdinov B., Hagiya K., Noguchi S., Ohmasa M., Ikeda N., Kusaka K. and Iishi K. (2002) - Low-temperature studies on the two-dimensional modulations in åkermanite-type crystals: $Ca_2MgSi_2O_7$ and $Ca_2ZnSi_2O_7$. *Physics and Chemistry of Minerals*, 29, 346-350.

Chavan S., Patwe S. and Tyagi A. (2003) - Bulk and lattice thermal expansion in $Ce_{1-x}Sr_xO_{2-x}$ ($0.0 \le x \le 0.10$). *Journal of Alloys and Compounds*, 360, 189-192.

Chavan S., Mathews M. and Tyagi A. (2004) - Phase relations and thermal expansion studies in the ceria-yttria system. *Journal of American Ceramic Society*, 87, 1977-1980.

Du J., Zeng H., Song L., Dong Z., Ma H., Guo G. and Huang J. (2003) - Synthesis and structure of a new polymorph $Ba_2CuSi_2O_7$. *Chinese Journal of Structural Chemistry*, 22, 33-36.

El Bali B. and Zavalij P. (2003) - Tetragonal form of barium cobalt disilicate, $Ba_2CoSi_2O_7$. *Acta Crystallographica*, E59, 59-61.

Haussühl S. and Liebertz J. (2004) - Elastic and thermoelastic properties of synthetic $Ca_2MgSi_2O_7$ (åkermanite) and $Ca_2ZnSi_2O_7$ (hardystonite). *Physics and Chemistry of Minerals*, 31, 565-567.

Hemingway B., Evans H., Nord G., Haselton H., Robie R. and McGee J. (1986) - Åkermanite: phase transitions in heat capacity and thermal expansion, and revised thermodynamic data. *Canadian Mineralogist*, 24, 425-434.

Hazen R. and Finger L. (1982) - Comparative crystal chemistry. Wiley, New York, 231pp.

Kaiser J. and Jeitschko W. (2002) - Crystal structure of the new barium zinc silicate $Ba_2ZnSi_2O_7$. *Zeitschrift für Kristallographie - New Crystal Structures,* 217(1), 25-26.

Kimata M. and Ii N. (1981) - The crystal structure of synthetic åkermanite, $Ca_2MgSi_2O_7$. *Neues Jahrbuch für Mineralogie, Monatshefte*, 1-10.

Körner R., Ricken M., Nölting J. and Riess I. (1989) - Phase transformations in reduced ceria: determination by thermal expansion measurements.

Journal of Solid State Chemistry, 78, 136-147.

Kusaka K., Hagiya K., Ohmasa M., Mukai M., Iishi K. and Haga N. (2001) - Determination of structures of $Ca_2CoSi_2O_7$, $Ca_2MgSi_2O_7$ and $Ca_2(Mg_{0.55}Fe_{0.45})Si_2O_7$ in incommensurate and normal phases and observation of diffuse streaks at high temperature. *Physics and Chemistry of Minerals*, 28, 150-166.

Larson A. and Von Dreele R. (1988) - General Structure Analysis System (GSAS). Los Alamos National Laboratory Report (LAUR 86-748), Los Alamos, NewMexico, 224pp.

Malinovskii Yu A. (1984) - Crystal structure of $Ba_2CuSi_2O_7$. *Soviet Physics Doklady*, 29, 706-708.

Mathews M., Ambekar B. and Tyagi A. (2000) - Bulk and lattice thermal expansion of $Th_{1-x}Ce_xO_2$. *Journal of Nuclear Materials*, 280, 246-249.

McConnell J., McCammon C., Angel R. and Seifert F. (2000) - The nature of the incommensurate structure in åkermanite, $Ca_2MgSi_2O_7$, and the character of its transformation from the normal structure. *Zeitschrift für Kristallographie*, 215, 669-677.

Merlini M., Gemmi M. and Artioli G. (2005) - Thermal expansion and phase transitions in åkermanite and gehlenite. *Physics and Chemistry of Minerals*, 32, 189-196.

Merlini M., Gemmi M., Cruciani G. and Artioli G. (2008) - High-temperature behaviour of melilite: in situ X-ray diffraction study of gehlenite–åkermanite–Na melilite solid solution. *Physics and Chemistry of Minerals*, 35, 147-155.

Merlini M., Gemmi M., Hanfland M. and Crichton W. (2009) - High-pressure behaviour of åkermanite and gehlenite and phase stability of the normal structure in melilites. *American Mineralogist*, 94, 704-709.

Riester M. and Böhm H. (1997) - Phase transition of modulated Co-åkermanite, $Ca_2CoSi_2O_7$. *Zeitschrift für Kristallographie*, 212, 506-509.

Röthlisberger F., Seifert F. and Czank M. (1990) - Chemical control of the commensurate-incommensurate phase transition in systematic melilites. *European Journal of Mineralogy*, 2, 585-594.

Sameshima S., Ichikawa T., Kawaminami M. and Hirata Y. (1999) - Thermal and mechanical properties of rare earth-doped ceria ceramics. *Materials Chemistry and Physics*, 61, 31-35.

Shimizu M., Kimata M. and Iida I. (1995) - Crystal structure of $Ba_2MgSi_2O_7$ melilite: the longest tetrahedral Mg–O distance. *Neues Jahrbuch für Mineralogie, Monatshefte*, 39-47.

Shuk P. and Greenblatt M. (1999) - Hydrothermal synthesis and properties of mixed conductors based on $Ce_{1-x}Pr_xO_{2-\delta}$ solid solutions. *Solid State Ionics*, 116, 217-223.

Toby H. (2001) - EXPGUI, a graphical user interface for GSAS. *Journal of Applied Crystallogr*aphy, 34, 210-213.

Webb S., Ross C. and Liebertz J. (1992) - Thermal expansion and spontaneous strain associated with the Normal-Incommensurate phase transition in melilites. *Physics and Chemistry of Minerals*, 18, 522-525.

Yang H., Hazen R., Downs R. and Finger L. (1997) - Structural change associated with the incommensurate-normal phase transition in åkermanite, $Ca_2MgSi_2O_7$, at high pressure. *Physics and Chemistry of Minerals*, 24, 510-519.

Submitted, October 2010 - Accepted, January 2011